Self-consistent modeling of the dynamic evolution of magnetic island growth in the presence of stabilizing electron-cyclotron current drive

Ioanna Chatziantonaki[1]**, Christos Tsironis**[1,2]**, Heinz Isliker**[1] **and Loukas Vlahos**[1]

[1] Department of Physics, Aristotle University of Thessaloniki, 54 124 Thessaloniki, Greece
[2] School of Electrical and Computer Engineering, National Technical University of Athens, 157 73 Athens, Greece

E-mail: ctsironis@astro.auth.gr

Abstract
The most promising technique for the control of neoclassical tearing modes in tokamak experiments is the compensation of the missing bootstrap current with an electron-cyclotron current drive (ECCD). In this frame, the dynamics of magnetic islands has been studied extensively in terms of the modified Rutherford equation (MRE), including the presence of a current drive, either analytically described or computed by numerical methods. In this article, a self-consistent model for the dynamic evolution of the magnetic island and the driven current is derived, which takes into account the island's magnetic topology and its effect on the current drive. The model combines the MRE with a ray-tracing approach to electron-cyclotron wave-propagation and absorption. Numerical results exhibit a decrease in the time required for complete stabilization with respect to the conventional computation (not taking into account the island geometry), which increases by increasing the initial island size and radial misalignment of the deposition.

1. Introduction

An important issue for the ITER design, which is under careful investigation, is the stabilization of neoclassical tearing modes (NTMs) by using an electron-cyclotron current drive (ECCD). NTMs inhibit the optimal operation of tokamak devices because the generated magnetic islands, on surfaces with a rational safety factor value $q = m/n$, taper the plasma energy and angular momentum leading to a gradual loss of confinement and finally disruption [1, 2]. It is estimated that NTMs will be dynamically unstable in ITER, due to the high plasma pressure scenarios to be envisaged for achieving effective fusion results, and that both the 2/1 and 3/2 modes will be present [3]. The successful control of NTMs with ECCD has been demonstrated in large-scale experiments like AUG, DIII-D and JT-60U [4, 5]; these results form the basis for designing a corresponding control system for ITER.

There has been a lot of research on the properties of the NTM stabilization by EC waves, mainly investigating the effect of localized wave power deposition and current drive on the magnetic island growth (reviews on this topic are [3] and [6]). The evolution of ECCD-driven magnetic islands has been extensively analyzed in terms of the modified Rutherford equation (MRE): a modification of the Rutherford equation for classical tearing modes with the inclusion, among other physics, of the bootstrap current and the external current drive [4, 7]. It has been understood in both theory and experiment that, in order to succeed in a more effective mode stabilization, the cyclotron resonance should be highly localized around the island's O-point and the direction of the driven current should be aligned with the equilibrium bootstrap current.

The common knowledge that NTM stabilization will probably be a major issue in ITER (and maybe also in DEMO) has led to an effort of improving the modeling of magnetic

island dynamics in the presence of a stabilizing ECCD, both on a general theoretical basis as well as in terms of simulations oriented to specific devices, so that the goal of successful validation with experiments can be reached. Many effects that may play a role in the stabilization effort and that were excluded from the earlier exploratory research, like e.g. local electron transport, diamagnetic rotation [8], wave-induced electric field ([9], with comments by [10]), edge turbulence [11] and EC beam misalignment, as well as the possible advantage of early ECCD application [12], are currently being analyzed through the use of different techniques.

Regarding the modeling of ECCD, a variety of methods are available for computing the wave propagation, resonant absorption and driven current. For the propagation, one mainly bases it on the asymptotic methods originating from geometric optics [13]. In ray tracing, canonical equations provide the position and the wavenumber along the ray trajectory in terms of the derivatives of the dispersion relation [14]. The rays do not interact among themselves, therefore wave effects like diffraction are not properly accounted for. In quasi-optics, a beam is simulated as a set of interacting rays, therefore the basic wave effects are retained [15], whereas pWKB beam tracing is a more convenient description, based on a combination of ray tracing with a set of functions for the beam width and the wavefront curvature [16]. The computation of the wave damping breaks down to evaluating the linear absorption coefficient along the ray path [17], whereas the current drive may be calculated analytically with the linear adjoint method [18]. There are a number of advanced codes implementing the above schemes and the results, in some cases, are in sufficient agreement with the experiment [19].

In almost all the codes that simulate ECCD-based NTM stabilization, the analysis of the wave evolution is done in the unperturbed magnetic configuration, assuming sufficient alignment of the EC resonance with the island's O-point on the flux surface of interest, yet ignoring effects from the island's topology. This approach does not introduce an error in the computation of the ray propagation due to the smallness of the amplitude of the magnetic perturbation. However, islands bring up significant changes in the magnetic topology and the plasma profiles in comparison to the axisymmetric case: the different nesting of the flux surfaces and the flattening of the pressure profile within the island may play a crucial role in the wave deposition [20]. Moreover, the ECCD efficiency in the presence of an island has been shown to be much different from the axisymmetric case, leading to different estimates for the minimum current required for stabilization [9, 21].

There have been many efforts to introduce effects owed to the island geometry in the MRE formalism, since, in general, changes to the island shape are neglected by considering only the dominant harmonic of the perturbed flux. In this direction, the MRE has been reformulated to include a model for asymmetric island deformation [22], with the goal to ascertain the additional requirements that an ECCD-based NTM control system must satisfy if the magnetic islands undergo deformations induced e.g. by a sheared viscous flow. The results show that such deformations nonlinearly affect the time-scale of the island growth and can introduce a severe reduction in the ECCD control capability. This may have consequences for the localization of the beam around the O-point and the estimate of the minimum power needed for island quench.

A different modeling option for improving the accuracy in the description of the island topology within the frame of the MRE is to introduce a set of device-dependent parameters as multipliers of each term and determine these by fitting the MRE solution to experimental results from specific devices [6, 23]. In this fashion, deviations owed to simplifications in the modeling (like the adoption of cylindrical geometry in some cases) are minimized. The main results indicate that in ITER, if the wave beam and the island's O-point are sufficiently aligned, the minimum wave power required to stabilize the 2/1 and 3/2 modes is always within the capabilities of the planned EC system. This suggests that the most challenging task for NTM control in ITER might be the optimization of the alignment between the ECCD injection and the island motion.

The effect of the island's topology on the ECCD is studied also in terms of electron transport models. Simulations of the 2/1 NTM have been performed using the transport code TOPICS [24], combined with an experimentally fitted version of the MRE; the temporal evolution of the island's width, as observed in JT-60U, was found to be well reproduced by the model. The simulation also showed that increasingly precise injection is required for smaller EC power and that the allowable error in the ECCD location does not increase significantly, even for large EC wave power. These results are similar to the ones from DIII-D for a 3/2 NTM [25]. In addition, the TOPICS simulation predicts that the ECCD deposition width has a strong effect on the NTM control. This has experimentally been demonstrated in AUG, where it has been shown that narrow ECCD deposition could stabilize a NTM more effectively [5].

The Monte-Carlo method has been applied in the study of the characteristics of ECCD in the magnetic island as a test-particle problem in the island topology, including Coulomb collisions and the EC quasilinear diffusion process [21]. The driven current was found to remain localized within the helical flux tube and its profile tended to have a peak around the O-point, whereas the ECCD efficiency was computed to be larger than in the axisymmetric case. The enhancement of the current occurs because the resonant electrons are well-confined in the smaller volumes defined by the island, despite the nonlinear effect introduced by high-power density [26]. In such cases, where the control is achieved by a current density driven around the O-point, the required power can be significantly reduced.

A self-consistent treatment of the wave-island interaction has been made with the numerical code NIMROD [27], by augmenting the code with a quasilinear model for the basic EC wave physics to a closed set of RF-MHD equations [28]. The investigation of the effect of ECCD on the dynamical behavior of NTMs demonstrated the complete suppression of initially saturated 2/1 and 3/2 modes by the application of toroidally symmetric ECCD. Also demonstrated were the consequences of the shifting of the mode flux surface in response to the injected current and of the spatial ECCD misalignment. These effects cannot be easily described by

models based on the MRE. In a further development, the incorporation of the ability to use data from ray tracing codes in the NIMROD simulations, in order to determine the amplitude and spatial localization of the induced electromotive forces, has been theoretically established in terms of an advanced RF-MHD model [29].

In this paper, a self-consistent computation of the dynamic evolution of the NTM growth in the presence of a stabilizing ECCD is performed, on the basis of linear wave–particle physics and including the effect of island geometry on the ECCD, as presented in recent work [20]. The connection of the effect of the island topology on the EC wave propagation and the resonant electron transport with the NTM dynamics, through the modification of the ECCD, is formulated by coupling the generalized Rutherford model with a ray-tracing solver. The geometric effect is introduced in this approach in terms of a fitting function that connects the island's width and the driven current density, which is determined with the ray-tracing code. Then, the MRE is solved as a function of time, with the instantaneously required values of the ECCD density being given through the mentioned and pre-computed fitting function.

The structure of the paper is as follows: in section 2, the self-consistent numerical model is presented with a synopsis of the theory behind it, focusing on the coupling of the wave-field solution with the MRE; in section 3, the numerical results are presented and analyzed for the different cases studied. Finally, in section 4, the main results are summarized and the limitations of our model are discussed.

2. Overview of the self-consistent model

Keeping the focus on the effect of island geometry on ECCD deposition, the most important aspects to be considered are the influence of the helical magnetic field on the wave propagation and on the determination of the resonance region, the flattening of the radial profiles of the plasma electron density and temperature within the island region and the structure of the volumes of the perturbed flux surfaces into which the wave power is deposited. The simulation tool we use for the computation of the EC propagation in a magnetic configuration that includes islands is the ray-tracing code CODERAY [20], whereas the connection of the results for the wave to the dynamics of the NTM suppression is made by solving numerically the MRE.

In the ray-tracing asymptotic technique, which stems from geometric optics theory, the propagation of waves is formulated in terms of a set of ordinary differential equations (ODEs), which may be integrated by means of a standard numerical solver and therefore are simpler to tackle than the (partial differential) Helmholtz equation. The canonical equations for the ray propagation in this framework are [14, 30]

$$\frac{\mathrm{d}\boldsymbol{k}}{\mathrm{d}t} = -\frac{\partial\omega}{\partial\boldsymbol{r}}, \qquad (1a)$$

$$\frac{\mathrm{d}\boldsymbol{r}}{\mathrm{d}t} = \frac{\partial\omega}{\partial\boldsymbol{k}}, \qquad (1b)$$

where the ray position $\boldsymbol{r}$ and the wave vector $\boldsymbol{k}$ are canonical variables and the wave frequency ω plays the role of the Hamiltonian. The solution of (1a) and (1b) determines the propagation in the plasma as a function of time, with a characteristic wave period time-scale. A new independent variable τ can be introduced, such that the equations take a form where t is replaced by τ and ω is replaced by a new Hamiltonian $\mathcal{H}$ that is the solvability condition of the dispersion relation viewed as a function of $(\boldsymbol{r}, \boldsymbol{k})$. With $\boldsymbol{\epsilon}^h$, the Hermitian part of the plasma dielectric tensor and c the light speed in a vacuum, we have

$$\mathcal{H} = \det\left[\left(\frac{\omega}{c}\right)^2\left(-k^2\boldsymbol{I} + \boldsymbol{k}\boldsymbol{k}\right) + \boldsymbol{\epsilon}^h\right]. \qquad (2)$$

This formalism is most appropriate in the case of monochromatic wave propagation in stationary plasma, because it provides a relation of the integration step with the time, which is parametric-dependent only on the frequency; therefore, the time dependence can be further neglected. Assuming cold plasma propagation, one may adopt the cold plasma dielectric tensor [30], which gives the final expression for the Hamiltonian used here (for more information on the wave code, see [20]).

In the context of geometric optics, the wave propagation is a zero-order process, whereas the absorption and, consequently, the driven current are described by first-order equations. The wave absorption is computed along the ray path in terms of the imaginary part of the wave vector, as determined from the dispersion relation [17]. The evolution of the absorbed wave power P_{abs} is then given by

$$\frac{\mathrm{d}P_{\mathrm{abs}}}{\mathrm{d}\tau} = -2\mathrm{Im}(\boldsymbol{k})\cdot\boldsymbol{v}_g(P_0 - P_{\mathrm{abs}}), \qquad (3)$$

where $\boldsymbol{v}_g$ is the group velocity and P_0 is the injected wave power. With the absorbed power along the ray path known, the power $\mathrm{d}P_{\mathrm{abs}}$ deposited in a small radial interval can be calculated from (3); a division by the volume $\mathrm{d}V_{\mathrm{abs}}$ contained between the two flux surfaces enclosing the radial interval gives the absorbed power density. The total driven current I_{CD} over the absorbed power defines the current drive efficiency ζ_{CD} (r_{maj} is the major plasma radius)

$$\zeta_{\mathrm{CD}} = 2\pi r_{\mathrm{maj}}\frac{I_{\mathrm{CD}}}{P_{\mathrm{abs}}}. \qquad (4)$$

Following [18], the ECCD efficiency is computed in terms of the linear adjoint method, based on a Green's function formulation with the magnetic field approximated as a square well, in order to obtain an analytic solution; it includes the effects of trapped particles, ion–electron collisions and the spatial variation of the collision operator.

As an input to the wave solver, the magnetic field topology and the radial profiles of the electron density/temperature of the plasma must be provided. The non-axisymmetric magnetic configuration used here has been formulated as in [20]. To start with, the total magnetic field is expressed as

$$\boldsymbol{B} = \frac{1}{r}\frac{\partial\psi_t}{\partial r}\hat{e_r} + \frac{1}{R}\frac{\partial\psi_p}{\partial r}\hat{e_\theta} - \frac{1}{rR}\left(\frac{\partial\psi_p}{\partial\theta} + \frac{\partial\psi_t}{\partial\varphi}\right)\hat{e_\phi}, \quad (5)$$

with ψ_t, ψ_p the toroidal and poloidal flux functions, r, θ, φ the radial, toroidal and poloidal coordinates with unit base vectors $\hat{e}_r$, $\hat{e}_\theta$, $\hat{e}_\varphi$ and with $R = r_{\mathrm{maj}} + r\cos\theta$. For the axisymmetric part of the magnetic field, corresponding to the background equilibrium, the expression used is the one known as the 'vacuum magnetic field'

$$B_{t0}(r,\theta) = \frac{B_0}{1 + \epsilon_A(r)\cos\theta}, \tag{6a}$$

$$B_{p0}(r,\theta) = \frac{\epsilon_A(r)}{q(r)} B_{t0}(r), \tag{6b}$$

where B_{t0}, B_{p0} are the toroidal and poloidal components, respectively, B_0 the toroidal field on the magnetic axis, $\epsilon_A(r) = r/R_0$ the inverse aspect ratio and $q(r) = \mathrm{d}\phi/\mathrm{d}\theta$ is the safety factor, chosen as a monotonically increasing rational function, see [20]. The flux functions ψ_{t0}, ψ_{p0} corresponding to the fields can be calculated from the relations $\partial_r\psi_{t0} = rB_{t0}$ and $\partial_r\psi_{p0} = RB_{p0}$. The local magnetic field structure of the island is described by a perturbation ψ_{p1} to the poloidal flux, $\psi_p = \psi_{p0} + \psi_{p1}$, with

$$\psi_{p1}(r,\theta,\phi) = \varepsilon_{mn}(r)\cos(m\theta - n\phi), \tag{7}$$

see e.g. [31], where ε_{mn} is the perturbation strength and m, n are the mode numbers of the NTM. For an implementation of the NTM topology, one has to specify $\varepsilon_{mn}(r)$, and, as described in detail in [20], we use the low-order approximation of [32] to the self-consistent expression given in [33],

$$\psi_{p1} = -\frac{r}{m}\varepsilon_{mn}^{(0)}\left(1 + \frac{r - r_s}{\alpha_\pm}\right)\cos(m\theta - n\phi), \tag{8}$$

with $\alpha_\pm$ the slopes and r_s the radius of the resonant surface, determined through the equation $q(r_s) = m/n$.

Apart from the changes in the magnetic topology, an excited NTM causes the plasma pressure to assume a constant value inside the separatrix of the island chain. This flattening in the pressure profile leads in turn to a flattening in the electron density and temperature profiles. In order to model this alteration of the plasma profiles, we assume the density and temperature profiles to be parabolic functions outside the island, as in the unperturbed case, to be constant within the island region, to be equal to the density and temperature values at the outer island boundary and to be continuous at the inner island boundary (see [20] for details).

For computing the power absorption in the presence of the island, calculation of the plasma volume between two adjacent flux surfaces is required. Again following [20], the total volume V_{abs} contained inside a flux surface is

$$V_{\mathrm{abs}} = -\frac{1}{n}\int_0^{2\pi n}\int_{\xi_1}^{\xi_2}\int_{r_1}^{r_2}\left(r_{\mathrm{maj}} + r\cos\theta\right)r\,\mathrm{d}r\,\mathrm{d}\xi\,\mathrm{d}\theta, \tag{9}$$

with $\xi = m\theta - n\phi$ the helical angle in the direction transverse to the line through the island's O-point and r_1, r_2, ξ_1, ξ_2 the integration limits. The definition of the integration limits, as given in [20], requires an analytical labeling Ω of the flux surfaces in the island region. This expression has been derived in [20] as

$$\Omega = \frac{1}{2}(r - r_s)^2 + \frac{r}{r_s}\Omega_s\left(1 + \frac{r - r_s}{\alpha_\pm}\right)\cos(\xi), \tag{10}$$

with

$$\Omega_s = \frac{r_s\varepsilon_{mn}^{(0)}}{m\,r_{\mathrm{maj}}\left(\partial_{rr}\psi_{p0}\right)\big|_{r_s}} \tag{11}$$

the value of Ω on the separatrix; the island half-width $W_{1/2}$ approximately is

$$W_{1/2} = \sqrt{\frac{2r_s\varepsilon_{mn}^{(0)}}{m\,r_{\mathrm{maj}}\left(\partial_{rr}\psi_{p0}\right)\big|_{r_s}}}. \tag{12}$$

Having these at hand, along with the ray-tracing data, the absorbed power per unit volume can be evaluated as

$$\frac{\mathrm{d}P_{\mathrm{abs}}}{\mathrm{d}V_{\mathrm{abs}}} = \frac{\mathrm{d}P_{\mathrm{abs}}}{\mathrm{d}\tau}\left(\frac{\mathrm{d}V_{\mathrm{abs}}}{\mathrm{d}\tau}\right)^{-1}. \tag{13}$$

The established model for the dynamic evolution of the NTM is the MRE, which is based on a generalization of the classical Rutherford equation for tearing modes [3, 7]. In the case of classical tearing modes, only the Ohmic current contributes, whereas for NTMs, other currents that flow in the island region, as appearing in neoclassical transport, need to be accounted for, the most important of which is the bootstrap current. In this context and with the inclusion of the stabilizing ECCD, the MRE becomes [6]

$$\frac{\tau_r}{r_s}\frac{\mathrm{d}W}{\mathrm{d}t} = r_s\Delta_\beta' = r_s\left(\Delta' + \Delta_{\mathrm{BS}}' + \Delta_{\mathrm{CD}}'\right), \tag{14}$$

where W is the full island width, $\tau_r = 0.82\mu_0 r_s^2/\eta_p$ the resistive time-scale of the plasma (η_p the plasma resistivity), Δ' the neoclassical stability index, including the classical index and a term connected to the nonlinear island saturation, Δ_{BS}' the stability index corresponding to the bootstrap current and Δ_{CD}' the term which represents the stabilizing effect of the driven current. These stability indices are given as [1, 6]

$$\Delta' = -\frac{m}{r_s} - \frac{W}{2.44r_{\mathrm{min}}^2}, \tag{15a}$$

$$\Delta_{\mathrm{BS}}' = \frac{\sqrt{\epsilon_A}\beta_P}{W}\frac{L_q}{L_p}\left(\frac{W^2}{W^2 + W_{\mathrm{d}}^2} + \frac{W^2}{W^2 + 28W_{\mathrm{b}}^2} - \frac{W_{\mathrm{pol}}^2}{W^2}\right), \tag{15b}$$

$$\Delta_{\mathrm{CD}}' = -\frac{16}{\pi}\frac{\mu_0 L_q}{B_\theta}\frac{1}{W^2}I_{\mathrm{CD}}\eta_{\mathrm{CD}}U(t - t_{\mathrm{CD}}^{\mathrm{on}}). \tag{15c}$$

In the above, r_{min} is the minor radius, $\epsilon_A = r_{\mathrm{min}}/r_{\mathrm{maj}}$ is the aspect ratio of the tokamak, β_P is the ratio of the plasma and magnetic pressures, L_q and L_p are the shear lengths of the safety factor and the plasma pressure, $t_{\mathrm{CD}}^{\mathrm{on}}$ is the time when the ECCD is turned on (with U the Heaviside step function [34]), I_{CD} is the driven current (η_{CD} is defined below) and W_{d}, W_{b} and

W_{pol} are characteristic threshold values for the island width: W_d is the critical width for classical destabilization, W_b is the width below which banana orbits contribute significantly to the bootstrap current and W_{pol} is the width below which the current generated in response to the diamagnetic island rotation is significant (for more details on the physics of the different parameters and terms see [1, 3, 35] and the references therein).

In the computation of the term Δ'_{CD}, the total driven current is expressed in terms of the current density as $I_{CD} = \pi^{3/2} r_s d_{CD} j_{CD}$, where j_{CD} is assumed to have a Gaussian radial profile around the O-point with peak value j_{CD0} and width d_{CD}

$$j_{CD} = j_{CD0} \exp\left[-\frac{(r - r_s - r_{mis})^2}{d_{CD}^2}\right], \qquad (16)$$

and r_{mis} denotes a small distance of radial misalignment between the deposition center and the O-point. The efficiency of the ECCD injection in stabilizing the NTM is described by the factor η_{CD} appearing in (15a)–(15c). η_{CD} is a measure of the geometrical optimization of the deposition on the basis of the ECCD radial profile width as compared to the island width (not to be confused with the current-drive efficiency ζ_{CD}, given in (4)). This factor, among other things, depends heavily on the synchronization of the island motion with the wave power constancy or modulation. For locked islands, stabilization is possible only if the O-point position is geometrically accessible to the EC system and no power modulation is required. When the islands rotate, conventionally Δ'_{CD} should be obtained by averaging (16) over the rotation period, in order to assess properly the distribution of the wave power over the different island phases. In our model, we have assumed that: (*a*) for locked modes, the EC deposition around the O-point is feasible and (*b*) for rotating modes, the power is modulated exactly at the island rotation frequency and the power-on phase is exactly centered around the O-point passage through the beam. In this framework, η_{CD} has the form [23]

$$\eta_{CD} = 0.07\left(\frac{W}{d_{CD}}\right)^2 + \left[0.34 - 0.07\left(\frac{W}{d_{CD}}\right)^2\right]$$
$$\times \left[\frac{0.3W}{d_{CD}} U\left(2 - \frac{W}{d_{CD}}\right) + \exp\left(-\frac{d_{CD}}{W}\right) U\left(\frac{W}{d_{CD}} - 2\right)\right]. \qquad (17)$$

In including the current drive modification caused by the island into the NTM dynamics self-consistently, the direct coupling of the MRE with the ray-tracing algorithm based on (1*a*) and (1*b*), with time as the common independent variable, exhibits the problem of the vastly different time-scales of evolution: in ITER, the wave period T is of the order of at most 10^{-10} s, whereas the resistive time-scale is of the order of at least 10^{-4} s. It becomes obvious that the island evolution, being a 'slow' process, will not be affected by wave effects on a time-scale comparable to T, whereas the 'fast' wave propagation could potentially also be affected on a time-scale of the order of t_r. Since it would be obligatory, in order to obtain a physically consistent solution, to time-step the problem on the slow time-scale, an inefficiency in the computational scheme would result.

In order to reduce the computational burden for treating the problem, we evolve the plasma instability process on the t_r time-scale during the EC wave propagation. For better efficiency, we actually progress only the MRE and, at each time step (which is comparable to t_r), we compute the radial profile of the ECCD with the ray-tracing code, using the instantaneous value of the island width for determining the magnetic field perturbation and other related parameters. The resulting new value of the driven current density, which now includes the modification caused by the change of the island width, is then provided back to the MRE in order to compute the next step that yields the new island width, and so on. Non-strictly speaking, this defines a self-consistent model for the evolution of the magnetic island width and the ECCD profile.

One may further disengage from running the wave code at each time-step of the MRE: since the problem setup for the wave evolution is linear, as the propagation/absorption is treated in terms of a linear dielectric response tensor and the current drive is computed with the linear adjoint method, what is practically needed for including the effect of the island on the ECCD is an analytic or tabular function connecting W and j_{CD}. According to (15a)–(15c) and (17), in order to express the relation $j_{CD} = f(W)$ for a specific injection setup (P_0, θ_l, ϕ_l), one needs to determine, via the ray-tracing data, the dependence of j_{CD0} and d_{CD} on W (r_s depends only on the q-profile). In this sense, one can use the wave code to compute the parameters of the driven current for many different W values in order to build a table of the corresponding j_{CD0} values; then, in evolving the MRE, at a certain time t when the island width is W, one computes the required value of j_{CD0} by linear interpolation/extrapolation of the tabulated values.

3. Numerical results

This section contains the numerical results for the estimation of the effect of the magnetic topology on the NTM dynamics via the alteration of the driven current, using the self-consistent model previously described. As described above, we incorporate the island geometry via a set of tabulated values connecting the island width and the driven current density, which are computed by the ray-tracing code CODERAY. Thereafter, the MRF is solved numerically, with the required values of the ECCD being determined from the pre-computed and tabulated values of j_{CD0} versus W.

Regarding the characteristics of the stabilization process, especially its global efficiency and speed in both cases of locked and rotating islands, the important effects to be investigated here have to do with the following parameters: (a) the initial value of the island width, (b) the radial misalignment of the ECCD peak with respect to the O-point and (c) the specific time instant at which the wave power is turned on.

3.1. Ray tracing computations of ECCD

In ray-tracing computations, we use a magnetic equilibrium with islands, as generated by a NTM of order 3/2, in combination with the varying magnetic perturbation strengths
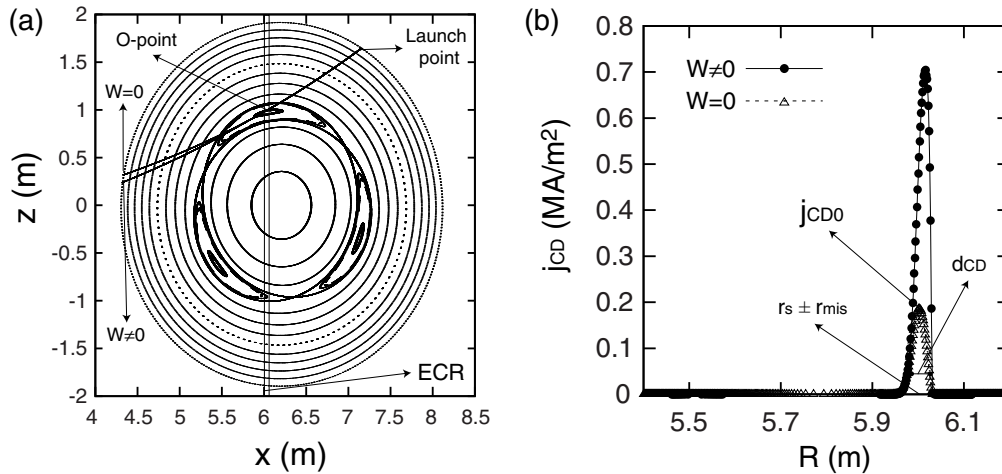
Figure 1. EC wave propagation and current drive, as computed by the ray-tracing code CODERAY, for the case of a $m/n = 3/2$ mode in ITER with $W_0 = 30$ cm (in comparison with the same computation performed in axisymmetric geometry): (a) poloidal projection of the ray propagation path, (b) radial profile of the ECCD density.

(and thus island widths); we also include the effect of the flattening of the plasma pressure profile (for details see [20]). The wave is launched from the outermost flux surface ($r = r_{min}$), at a poloidal angle such that the ray propagation targets extremely close to the O-point (the necessity for $r_{mis} \approx 0$ will be analyzed later on) and a toroidal magnetic field for which the EC resonance layer is located around the O-point. The plasma and wave parameters are the ones foreseen in ITER: the major and minor radii are $r_{maj} = 6.2$ m and $r_{min} = 1.9$ m, the magnetic field on the tokamak magnetic axis is $B_0 = 5.51$ T, the electron density and temperature follow parabolic profiles with values at the plasma center equal to $n_e(0) = 10^{20}$ m^{-3}, $T_e(0) = 10$ KeV and at the edge $n_e(r_{min}) = 10^{19}$ m^{-3}, $T_e(r_{min}) = 1$ KeV, the q-profile is also parabolic with $q(0) = 1$, $q(r_{min}) = 4$ (see [20]), the wave frequency is $\omega/2\pi = 170$ GHz (fundamental O-mode) and the initial wave power is $P_0 = 10$ MW.

An indicative result from the wave code is shown in figure 1, where, apart from the parameters mentioned above, the magnetic perturbation strength has a value such that the island width is $W_0 = 30$ cm. In figure 1(a), we show the projection of the ray path onto the poloidal plane in the presence of the NTM and also compare it to the corresponding path in the unperturbed equilibrium (i.e. in the absence of the mode). The injection angles of the EC wave beam are $\theta_l = -30°$ poloidally and $\phi_l = -5°$ toroidally. For the assumed profiles of B, q, n_e, T_e and the chosen value of ω, the layer of the EC resonance is located around $R = 6$ m, as marked in figure 1(a) with the narrow region between the two vertical lines. In figure 1(b), the radial profile of the ECCD density is visualized for the two cases, with and without a NTM present, respectively; here we just note that the obvious characteristic differences and effects have been analyzed and discussed in detail in [20].

The shape of the radial profile in figure 1(b) highly resembles a Gaussian function curve, which implies that fitting the profile data against the Gaussian function in equation (16) is appropriate. This fitting, provided that $r_{mis} \approx 0$ (as ensured during ray-tracing computations), yields the parameters j_{CD0}, d_{CD} for a given profile and value of W and that it has been

Table 1. The numerical values of j_{CD0} and d_{CD}, for different values of W (or ϵ_{32}), determined through a Gaussian fit to the ray-tracing data (ECCD profiles).

ϵ_{32}	W (m)	j_{CD0} (MA m^{-2})	d_{CD} (m)
0.000	0.0000	0.1102	0.019 04
0.012	0.1134	0.2123	0.019 84
0.015	0.1247	0.2216	0.019 85
0.017	0.1350	0.2283	0.019 91
0.020	0.1450	0.2368	0.020 02
0.023	0.1553	0.2451	0.020 16
0.026	0.1654	0.2528	0.020 23
0.029	0.1749	0.2614	0.020 33
0.032	0.1853	0.2732	0.020 47
0.036	0.1952	0.2864	0.020 58
0.039	0.2047	0.2986	0.020 66

repeated for varying values of W. The resulting data for the peak value and the $1/e$-width of the ECCD profile, as a function of the island width or the dimensionless magnetic perturbation amplitude, are given in table 1. The only parameter that has changed with respect to the above is $\phi_l = 0°$; in the first row the results for the unperturbed case $W = 0$ is included, in order to perform comparisons. The physical reason for the dependence of j_{CD0} and d_{CD} on W stems from the fact that, in the presence of the island, the wave power is deposited into volumes smaller than those in its absence, which in turn leads to larger values of the absorbed power density and the driven current. As the island width increases, so does the magnetic perturbation strength; the flux surface nesting in the interior of the island becomes more complicated, therefore this effect appears stronger. The dependence of d_{CD} on W is much weaker (the overall increase is 0.16 cm over a 20 cm increase of the island size), however it was included in the modeling for consistency reasons.

For practical reasons, instead of interpolating/extrapolating j_{CD0} and d_{CD} from the values of table 1 to arbitrary values of W, one may introduce appropriate functional forms $j_{CD0} = f_1(W)$ and $d_{CD} = f_2(W)$ and make them specific by fitting them to the tabulated values. Since the ECCD computation is done in

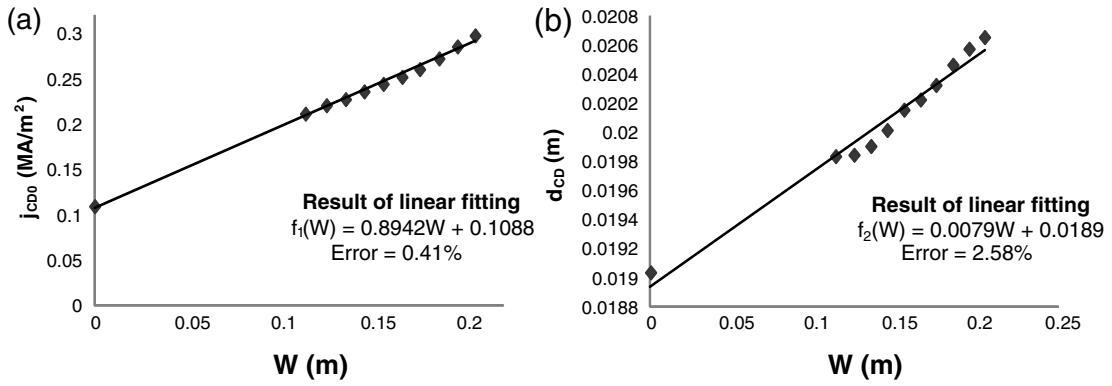**Figure 2.** Results of the linear fitting (least-squares method) to the tabulated values of (*a*) j_{CD0} and (*b*) d_{CD} in table 1, as a function of the island width.
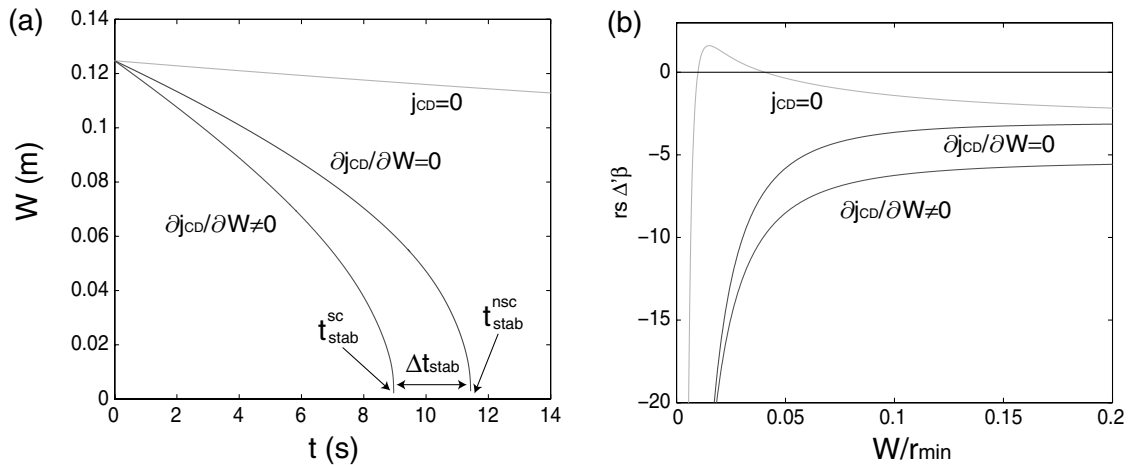

Figure 3. Self-consistent solution of the MRE for the case of a 3/2 mode in ITER with $W_0 = 12.47$ cm, in comparison with two cases of the non-self-consistent computation in axisymmetric geometry, namely in the presence and absence of ECCD, respectively: (*a*) time-evolution of the island width and (*b*) phase diagram of the MRE.

terms of the linear adjoint method, it is expected that the scaling of j_{CD0} and d_{CD} with W will be, in a good approximation, linear. Indeed, as shown in figure 2, the result of the linear fitting is very successful in both cases: the regression error for $f_1(W)$ is less than 1% and for $f_2(W)$ it is less than 3%. So, in the frame of the MRE evolution, we will use the fitted functions f_1 and f_2.

3.2. Solution of the MRE

In this section, the MRE is solved self-consistently by using the results on the current drive from the previous section and the results are analyzed in comparison to those from the non-self-consistent case in axisymmetric geometry. The parameters used here are the same as in the wave computations; the parameters specific to the MRE are chosen as $\beta_P = 0.5$, $L_q = L_p = 1$, $W_d = 0.01r_s$, $W_b = 0.02r_s$ and $W_{pol} = 0.015r_s$. The radius of the flux surface where the mode resides is found by solving the algebraic equation $q(r_s) = 3/2$; the ECCD density (peak value, width and misalignment) is given by the fitted functions f_1 and f_2 from the previous section. Concerning the results, we mostly focus on the time-domain signal (W versus t) and the phase diagram ($r_s\Delta'_\beta$ versus W/r_{min}).

In figure 3, the solution of the MRE for initial width $W_0 = 12.47$ cm and $t_{CD}^{on} = 0$ s, $r_{mis} = 1$ cm for the EC power is presented, in the cases of no ECCD applied ($j_{CD} = 0$), of ECCD applied and computed in the axisymmetric geometry ($\partial j_{CD}/\partial W = 0$) and of ECCD applied and computed self-consistently in the perturbed geometry ($\partial j_{CD}/\partial W \neq 0$). The evolution of $W(t)$, as seen in figure 3(*a*), reveals that the NTM is stabilized faster on the basis of the self-consistent computation. This occurs because the ECCD density, as computed in terms of the self-consistent model, is always larger than the one in the axisymmetric case, due to the geometric effect of smaller flux-surface volumes (see [20]), which ultimately leads to an enhancement of Δ'_{CD}. This can also be seen in figure 3(*b*), which is actually an imprint of the growth dynamics, and where the phase curve from the self-consistent model attains larger negative values than in the other two cases.

In the following, we will further investigate the deviation appearing in the computation of the time required for complete stabilization between the two models. As 'stabilization time' we define the time interval from the time-instant the mode that is affected by the EC control system till the nullification of the island width, which we denote by t_{stab}^{nsc} for the non-self-consistent computation and by t_{stab}^{sc} for the self-consistent one.

Table 2. Numerical values of the non-self-consistent and self-consistent computations of the stabilization time t_{stab}^{nsc}, t_{stab}^{sc} and their deviation Δt_{stab} in the case of a 3/2 NTM in ITER for different values of the initial width W_0 and for different combinations of t_{CD}^{on} and r_{mis}.

W_0 (m)		$t_{stab}^{nsc} - t_{stab}^{sc} = \Delta t_{stab}$ (s)	
0.1134	$9.436 - 5.978 = 3.458$	$12.359 - 7.766 = 4.593$	$27.798 - 17.124 = 10.674$
	$11.518 - 7.923 = 3.596$	$14.505 - 9.897 = 4.608$	$29.496 - 19.165 = 10.331$
0.1247	$11.432 - 7.067 = 4.365$	$14.866 - 9.138 = 5.728$	$32.410 - 19.751 = 12.659$
	$13.531 - 8.997 = 4.534$	$16.905 - 11.051 = 5.854$	$34.045 - 21.866 = 12.179$
0.1350	$13.369 - 8.107 = 5.262$	$17.273 - 10.442 = 6.831$	$36.622 - 22.167 = 14.455$
	$15.402 - 10.032 = 5.370$	$19.349 - 12.579 = 6.770$	$38.099 - 24.178 = 13.921$
0.1450	$15.348 - 9.153 = 6.195$	$19.704 - 11.737 = 7.967$	$40.709 - 24.534 = 16.175$
	$17.495 - 11.038 = 6.457$	$21.635 - 13.848 = 7.787$	$42.046 - 26.425 = 15.621$
0.1553	$17.482 - 10.272 = 7.210$	$22.291 - 13.109 = 9.182$	$44.903 - 26.955 = 17.948$
	$19.485 - 12.386 = 7.099$	$24.091 - 15.192 = 8.889$	$46.124 - 28.770 = 17.354$
0.1654	$19.640 - 11.393 = 8.247$	$24.901 - 14.481 = 10.420$	$48.983 - 29.338 = 19.645$
	$21.620 - 13.518 = 8.102$	$26.649 - 16.570 = 10.079$	$50.128 - 31.139 = 18.989$
0.1749	$21.739 - 12.467 = 9.272$	$27.401 - 15.799 = 11.602$	$52.791 - 31.586 = 21.205$
	$23.605 - 14.580 = 9.025$	$29.048 - 17.864 = 11.184$	$53.843 - 33.311 = 20.532$
0.1853	$24.096 - 13.671 = 10.425$	$30.188 - 17.261 = 12.927$	$56.914 - 34.019 = 22.895$
	$25.855 - 15.766 = 10.089$	$31.740 - 19.463 = 12.277$	$57.884 - 35.692 = 22.192$
0.1952	$26.390 - 14.840 = 11.550$	$32.884 - 18.673 = 14.211$	$60.803 - 36.334 = 24.469$
	$28.062 - 16.921 = 11.141$	$34.341 - 20.807 = 13.534$	$61.718 - 37.956 = 23.762$
0.2047	$28.634 - 15.977 = 12.657$	$35.497 - 20.036 = 15.461$	$64.498 - 38.550 = 25.948$
	$30.234 - 18.038 = 12.196$	$36.884 - 22.117 = 14.767$	$65.342 - 40.134 = 25.208$
r_{mis} (m)	0.00	0.01	0.02
t_{CD}^{on} (s)	0 (1st line for each W_0)	2 (2nd line for each W_0)	

The deviation may then be defined as follows

$$\Delta t_{stab} = t_{stab}^{nsc} - t_{stab}^{sc}, \qquad (18)$$

as illustrated also in the schematic representation in figure 3(*a*). The parameters expected to affect the form of the self-consistent solution and the deviation from the standard result in axisymmetric geometry are the initial width W_0, the time-instant t_{CD}^{on} and the maximum misalignment r_{mis}. In order to ascertain the effect of these parameters on the overall process, t_{stab}^{nsc}, t_{stab}^{sc} and Δt_{stab} have been computed for several values of W_0 and different combinations of t_{CD}^{on}, r_{mis}. The results of these computations are shown in table 2.

The concept of the stabilization time and its behavior as a function of the ECCD have been analyzed in previous studies (see e.g. [5, 6]); since our work emphasizes the difference appearing in the estimation of the stabilization time when the effect of the island topology is taken into account self-consistently, an extensive analysis of stabilization times will not be made here. Just to mention, as seen in table 2, the values of t_{stab} range from 9 to 65 s, depend mainly on W_0 and r_{mis}. The stabilization times computed are nearly the same as the ones presented in [6], where complete stabilization was found to occur roughly in a minute for the 3/2 NTM and less than the characteristic NTM growth time expected in ITER (around 100 s). In the modeling setup, the wave power may safely be considered to be active for all this time interval, since a realistic high-power ECRH pulse from the 1 MW gyrotron planned for ITER can last up to 400 s.

For each one of the six combinations of r_{mis} and t_{CD}^{on}, the time-lag Δt_{stab} is an increasing function of W_0, meaning that for initially larger islands, the self-consistent model predicts a faster stabilization of the mode. This is visualized in figure 4(*a*), where Δt_{stab} is plotted against W_0 for $t_{CD}^{on} = 0$

s and three different values of r_{mis}. The specific scaling occurs because the geometric effect on Δ'_{CD}, which results in the increase of the latter, becomes more important when the size of the island is larger. Furthermore, after a closer examination of table 2, the first impression is that the scaling of Δt_{stab} with W_0 does not depend on t_{CD}^{on}. The respective plot of Δt_{stab} versus W_0 is shown in figure 4(*b*), for $r_{mis} = 0.01$ m and two different values of t_{CD}^{on}. As a matter of fact, the time-instant t_{CD}^{on} just determines the island width in the beginning of the stabilization effort, which, for the values of t_{CD}^{on} occurring in the experiments (<2 s) and the slow evolution of the island when the ECCD is off (see figure 3), retains a value very close to W_0.

Contrary to the above, there is clearly a dependence of the scaling of Δt_{stab} with W_0 on r_{mis}. In figure 4(*a*), this appears in the form of a parametric up-shift of the scaling relation. This effect can be expected, because as r_{mis} increases, the quantity of deposited ECCD in the island region decreases and, whereas Δ'_{CD} decreases within each computation alone, the difference of Δ'_{CD} values coming from the self-consistent model and the standard computation continuously becomes larger. In this sense, and up to the relatively small values of r_{mis} for which the island ultimately still disappears ($W = 0$ is still reached, see below), i.e. where the definition of equation (18) still yields finite values for Δt_{stab}, this time lag is expected to increase with increasing r_{mis}.

An additional computation of Δt_{stab} for many different values of r_{mis} within the range occurring in experiments (<3 cm) was performed, keeping the initial width constant at $W_0 = 0.1247$ m and $t_{CD}^{on} = 0$ s. The results are plotted in figure 5(*a*) and, according to these, the increase of Δt_{stab} with increasing r_{mis} is obvious. The scaling has been followed up to $r_{mis} = 3$ cm because for larger values of the misalignment, the driven current is not optimized enough with the O-point position and the island does ultimately not disappear anymore.
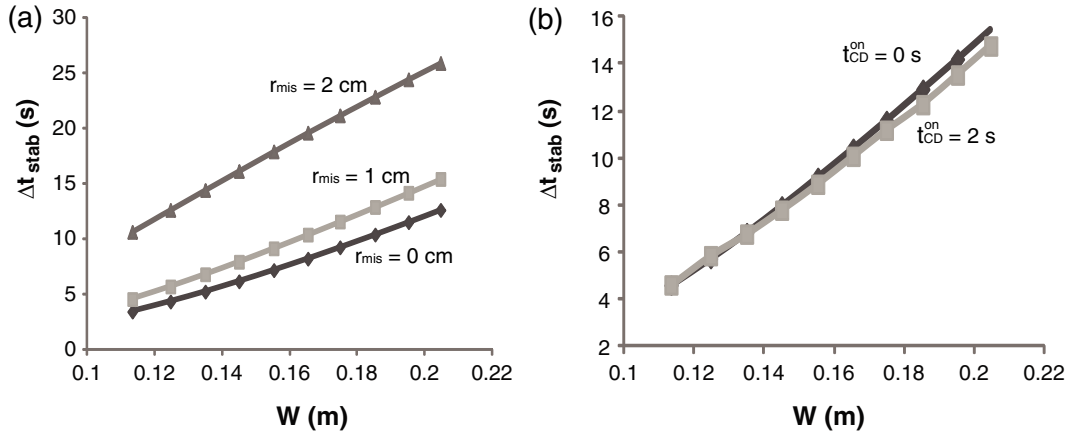
Figure 4. Dependence of the scaling of the time-lag Δt_{stab} with W_0 on $t_{\text{CD}}^{\text{on}}$ and r_{mis}: diagram of Δt_{stab} versus W_0 for (*a*) $t_{\text{CD}}^{\text{on}} = 0$ s and three different values of r_{mis}, (*b*) $r_{\text{mis}} = 0.01$ m and two different values of $t_{\text{CD}}^{\text{on}}$.

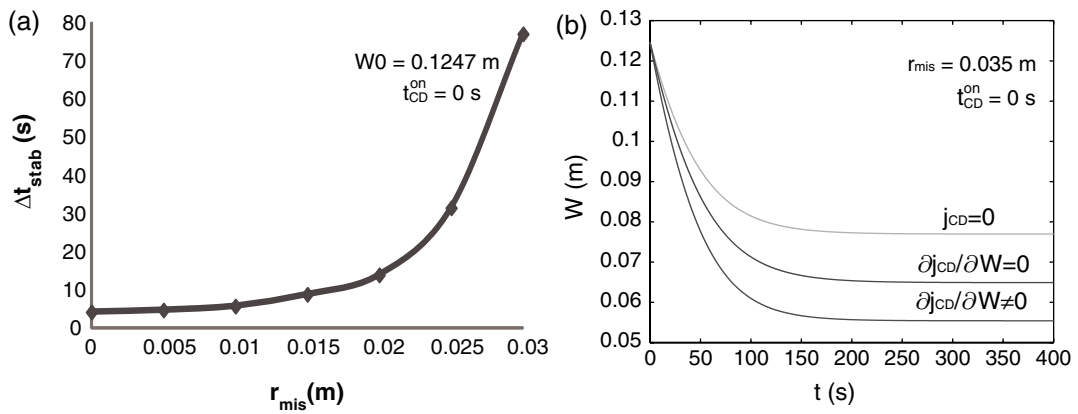**Figure 5.** Investigation of the dependence of the stabilization time-lag on the radial misalignment of the EC beam with the island center: (*a*) Δt_{stab} versus r_{mis} for $W_0 = 0.1247$ m and $t_{\text{CD}}^{\text{on}} = 0$ s, (*b*) W versus t for the same parameters and $r_{\text{mis}} = 0.035$ m.

This is verified in figure 5(*b*), a plot similar to figure 3, for the same parameters as in figure 5(*a*) and with $r_{\text{mis}} = 3.5$ cm, where the island stops shrinking at a width between 5.5 and 8 cm (depending on the simulation model). In this case, according to its definition, Δt_{stab} becomes infinite, a trend that already appears in figure 5(*a*).

The results presented so far on the deviation in the computed stabilization time between the two different models have been derived for a driven current based on the same injection power and geometry in all cases. A higher value of the current density achieved in terms of a larger value of P_0 would not yield a different picture for Δt_{stab}, since $\Delta'_{\text{CD}} \propto j_{\text{CD0}}$ and the ratio of the ECCD peak values, as computed by the two models, would not alter because the island geometry encountered by the ray has not changed much. On the contrary, a higher value of j_{CD0} achieved in terms of changing ϕ_l would result in a further increase of Δt_{stab} since the ratio of the peak values increases due to geometric effects [20].

4. Conclusion

In the context of the current drive requirements in modern fusion devices, including ITER and DEMO [36], a self-consistent model for the dynamic evolution of the NTM growth in the presence of a stabilizing ECCD has been performed,

assuming linear wave–particle interaction and including the effect of the island geometry on the ECCD. The model includes the effect of the helical magnetic perturbation on the propagation, the flattening of the plasma electron pressure within the island region and the volumes of the perturbed flux surfaces into which the wave deposits it power. In general, the inclusion of the island geometry in the NTM dynamics has the problem of the distant time scales for the wave and the instability. The most efficient treatment would be to evolve the plasma process at certain time slices during the NTM evolution and at each step to compute the ECCD profile with the ray-tracing code and provide the results back to the plasma process. Here, we used an even simpler setting and avoided using the wave code at each step; we numerically computed the current density for many values of the island width in advance and then solved the MRE, getting the required values of the current density from the tabulated results of the wave computation.

Numerical computations were performed for the mode 3/2, expected to be dominant in ITER, and parameters were chosen as relevant for a specific stabilization scenario, using the upper EC launcher. The main results are the following:

- The mode stabilization occurs faster in terms of the self-consistent model as compared to the conventional

estimation, since the corresponding term Δ'_{CD} in the MRE is always larger than the one in the axisymmetric case.

- The time-lag Δt_{stab} is an increasing function of the initial island width W_0, because the geometric effects on Δ'_{CD} are more important when the magnetic island is larger.
- The scaling of Δt_{stab} is almost independent of the EC turn-on time t_{CD}^{on}, since t_{CD}^{on} actually only causes a slight change of W_0.
- Δt_{stab} is an increasing function of r_{mis}, since for larger values of the misalignment Δ'_{CD} becomes larger with respect to the axisymmetric computation.

The fact that the stabilization process is computed to be faster when the island geometry is taken into account self-consistently in the ECCD suggests that the effect of the island geometry on the wave deposition is favorable for control, something that counteracts other known mechanisms that trim the ECCD efficiency and hamper the control effort, like e.g. quasilinear electron transport and wave beam broadening. The implementation of the island topology within the model allows for an accurate estimation of the ECCD effect on the NTM suppression. Revisiting the discussion in [20], it is verified that the enhanced ECCD peaking within the island may allow the use of less wave power than the one determined in axisymmetric geometry. This effect could serve in the direction of power economy, since less ECCD will be required for stabilization, provided that the coupling of power modulation with the frequency of island rotation is efficient.

A discussion of the limitations of our model is required. First, it has to be mentioned that the models for the wave propagation, absorption and current drive do not take into account diffraction or nonlinear wave–particle interaction. Second, the coupling of the wave propagation with the island growth dynamics has been realized in terms of a linear model of the scaling of the driven current with the island width, instead of a routine use of the wave code at each step of the mode evolution. This increases the computational efficiency and, within the linear plasma response context, it is sufficiently accurate. Third, the island dynamics were described in terms of a version of the modified Rutherford equation (MRE) that includes a simplification in the description of the classical stability index Δ', which, in principle, should be evaluated numerically by using the correct equilibrium current profile in a fully toroidal geometry. Finally, the stabilizing term Δ'_{CD} has been considered for the simple case where the island rotation is coped with by the ECRH system. The problem of asynchronism of the power modulation with the island rotation, as well as other relevant effects, are currently being studied in the community (see e.g. [8]).

Issues requiring further study include the modeling of modulated and broad ECCD, which have been studied only partially in this article, and the inclusion of the effect of edge density fluctuations as a mechanism for the undesired increase of the misalignment and/or the broadening of the EC beam. Also, a deeper study of the scaling laws of Δt_{stab} with W_0 and r_{mis} could provide valuable information in an effort to construct simple models for the effect of island topologies on the NTM dynamics. Other issues worthy of investigation are the modeling of the wave propagation with the plasma response computed in terms of the full particle dynamics in the non-axisymmetric fields and the effect of the ECCD on the background magnetic equilibrium, which may have been underestimated in the computations done up to now.

Acknowledgments

References

[1] Hegna C C and Callen J D 1997 *Phys. Plasmas* **4** 2940
[2] Wilson H R 2008 *Trans. Fusion Science Technol.* **53** 152
[3] LaHaye R J 2006 *Phys. Plasmas* **13** 055501
[4] Zohm H, Gantebein G, Leuterer F, Maraschek M, Poli E, Urso L and the ASDEX Upgrade Team 2007 *Plasma Phys. Control. Fusion* **49** B341
[5] Maraschek M 2012 *Nucl. Fusion* **52** 074007
[6] Urso L 2009 Modelling and experiments on NTM stabilisation at ASDEX Upgrade *PhD Thesis* Ludwig-Maximilians Universitaet Muenchen
[7] Rutherford P H 1973 *Phys. Fluids* **16** 1903
[8] Ayten B and Westerhof E 2012 *Phys. Plasmas* **18** 092506
[9] da S Rosa P R and Ziebell L F 2010 *Nucl. Fusion* **50** 115009
[10] Westerhof E 2011 *Nucl. Fusion* **51** 068001
[11] Tsironis C, Peeters A G, Isliker H, Strintzi D, Chatziantonaki I and Vlahos L 2009 *Phys. Plasmas* **16** 112510
[12] Lazaros A, Maraschek M and Zohm H 2007 *Phys. Plasmas* **14** 042505
[13] Bernstein I B 1975 *Phys. Fluids* **18** 320
[14] Friedland L and Bernstein I B 1980 *Phys. Rev.* A **22** 1680
[15] Mazzucato E 1989 *Phys. Fluids* B **1** 1855
[16] Pereverzev G V 1998 *Phys. Plasmas* **5** 3529
[17] Westerhof E 1989 Implementation of TORAY at JET *Technical Report* 89-183, FOM Rijnhuisen
[18] Cohen R H 1987 *Phys. Fluids* **30** 2442
[19] Prater R *et al* 2008 *Nucl. Fusion* **48** 035006
[20] Isliker H, Chatziantonaki I, Tsironis C and Vlahos L 2012 *Plasma Phys. Control. Fusion* **54** 095005
[21] Hamamatsu K, Takizuka T, Hayashi N and Ozeki T 2007 *Plasma Phys. Control. Fusion* **49** 1955
[22] Lazzaro E and Nowak S 2009 *Plasma Phys. Control. Fusion* **51** 035005
[23] Urso L, Maraschek M, Zohm H and the ASDEX Upgrade Team 2005 *J. Phys. Conf.* **25** 266
[24] Isayama A, Oyama N, Urano H, Suzuki T, Takechi M, Hayashi N, Nagasaki K, Kamada Y, Ide S, Ozeki T and the JT-60 Team 2007 *Plasma Phys. Control. Fusion* **47** 773
[25] LaHaye R J, Guenter S, Humphreys D A, Lohr J, Luce T C, Maraschek M, Petty C C, Prater R, Scoville J T and Strait E J 2002 *Phys. Plasmas* **9** 2051
[26] Kamendje R, Kasilov S V, Kernbichler W, Pavlenko I V, Poli E and Heyn M F 2005 *Phys. Plasmas* **12** 012502
[27] Sovinec C R, Glasser A H, Gianakon T A, Barnes D C, Nebel R A, Kruger S E, Plimpton S J, Tarditi A and Chu M S 2004 *J. Comput. Phys.* **195** 355
[28] Jenkins T G, Kruger S E, Hegna C C, Schnack D D and Sovinec C R 2010 *Phys. Plasmas* **17** 012502

[29] Jenkins T G and Kruger S E 2012 *Phys. Plasmas* **19** 122508

[30] Stix T H 1992 *Waves in Plasmas* 2nd edn (Berlin: Springer)

[31] Hazeltine R D and Meiss J D 1992 *Plasma Confinement* (Reading, MA: Addison-Wesley)

[32] Ren C, Callen J D, Gianakon T A, Hegna C C, Chang Z, Fredrickson E D, McGuire K M, Taylor G and Zarnstorff M C 1998 *Phys. Plasmas* **5** 450

[33] Militello F, Hastie R J and Porcelli F 2006 *Phys. Plasmas* **13** 112512

[34] Arfken G B and Weber H J 2005 *Mathematical Methods for Physicists* 6th edn (Amsterdam: Elsevier)

[35] Mikhailovskii A B 2003 *Contrib. Plasma Phys.* **43** 125

[36] Poli E, Fable E, Tardini G, Zohm H, Farina D, Figini L, Marushchenko N B and Porte L 2012 *Plasma Phys. Control. Fusion* **54** 101766